

In situ seriate droplet coalescence under an optical force

Jin Ho Jung · Kyung Heon Lee · Ghulam Destgeer ·
Kang Soo Lee · Hyunjun Cho · Byung Hang Ha ·
Hyung Jin Sung

Received: 27 August 2014 / Accepted: 25 November 2014 / Published online: 9 December 2014
© Springer-Verlag Berlin Heidelberg 2014

Abstract We demonstrated the induced coalescence of droplets under a highly accurate optical force control. Optical scattering and gradient forces were used to push and trap the droplets prior to coalescence within a microfluidic channel. The behavior of the droplets under the influence of an optical force was predicted using an analytical model that agreed well with the experimental data. The optical gradient force accelerated and decelerated the droplet within the laser beam region, and the drag force acting on the droplet was thoroughly characterized. A description of the optical trap was presented in terms of the momentum transfer from the photons to the droplet, effectively restricting droplet motion inside the microfluidic channel prior to coalescence. A phase diagram was plotted to distinguish between the three regimes of droplet coalescence, including the absence of coalescence, coalescence, and multiple coalescence events. The phase diagram permitted the laser power input and the net flow rate in the microfluidic channel to be estimated. This technique was applied to the synthesis of biodegradable gel microparticles.

Keywords Droplet coalescence · Optical force · Two-phase flow · Biodegradable gel · Droplet trapping

Jin Ho Jung and Kyung Heon Lee have contributed equally to this article.

Electronic supplementary material The online version of this article (doi:10.1007/s10404-014-1522-8) contains supplementary material, which is available to authorized users.

J. H. Jung · K. H. Lee · G. Destgeer · K. S. Lee · H. Cho ·
B. H. Ha · H. J. Sung (✉)
KAIST, Daejeon, Republic of Korea
e-mail: hjsung@kaist.ac.kr

1 Introduction

Numerous microfluidic platforms have been developed to enable chemical and biological investigations on the microscale (Whitesides 2006). Droplet-based microfluidic systems, for example, have been extensively studied and used for such experiments (Song et al. 2006; Teh et al. 2008; Baroud et al. 2010). These systems utilize immiscible fluids to generate picoliter-to-femtoliter-volume droplets that can isolate chemical reagents. The monodisperse microscale droplets provide a useful experimental tool that prevents sample diffusion, cross-contamination, or evaporation. As other advantages, reagent consumption is minimized and the miniaturized devices are inexpensive and suitable for bulk manufacturing (Song et al. 2006). A variety of research outcomes using droplet-based microfluidics have been reported, such as clinical diagnostics (Srinivasan et al. 2007), PCR enrichment (Tewhey et al. 2009), nanomaterial synthesis (Hoang et al. 2011), rapid screening of antibiotic toxicity (Churski et al. 2012), single cell studies (Um et al. 2012), and combinatorial synthesis (Theberge et al. 2012). The synthesis of biodegradable particles in a microfluidic system was demonstrated by diffusing cross-linking agent from the continuous phase to the droplets of an aqueous alginate solution (Chang and Su 2010). The particle synthesis process can be made simpler and more efficient by encapsulating the desired solutions within separate droplets and later coalescing these droplets to rapidly mix and cross-link the polymer.

Controlling the merging of droplets on a microfluidic chip is essential for conducting complex chemical or biological reaction procedures. A variety of methods for coalescing droplets have been developed based on the channel geometry (Hung et al. 2006; Tan et al. 2006; Niu et al. 2008; Christopher et al. 2009), thermo-capillary effects

(Baroud et al. 2007; Luong et al. 2012), and electro-coalescence (Ahn et al. 2006; Abate et al. 2010). Droplet coalescence can be achieved by introducing a laser beam into a microfluidic system. Such approaches are compatible with commonly used laboratory microscopy setups and are easy to implement. Optofluidic systems, known as an *optical tweezer*, have been used to manipulate microscale objects, including polymer beads, cells, and droplets (Ashkin and Dziedzic 1971; Grier 2003; Dholakia and Cizmar 2011). Several researchers have described the achievement of optofluidic droplet coalescence via optical vortex traps and laser-induced thermal gradients (Kotz et al. 2005; Lorenz et al. 2007). The facile manipulation of droplets was achieved in a variety of applications using optical trapping approaches. Microfluidic synthesis and diagnostics platforms require high-throughput assays that can process large amounts of data. A microfluidic system that can rapidly and continuously generate and coalesce droplets is in demand for use in parallel with other microfluidic operations.

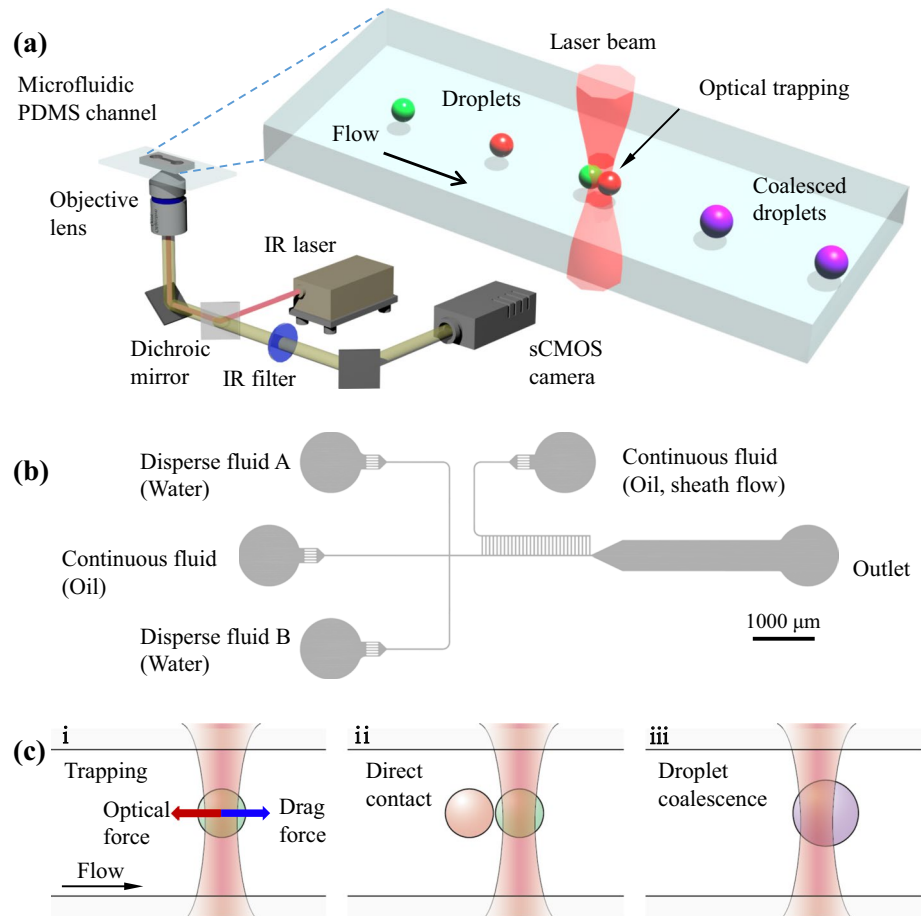
This paper describes the development of an optofluidic platform that can control and continuously coalesce droplets. Unlike previously reported techniques, our system is composed of a simple experimental setup, requires low-cost

chip fabrication, and achieves the highly controlled merging of droplets. The optical trapping and coalescence steps were modeled theoretically and demonstrated experimentally. Droplet generation and trapping were realized in a microfluidic channel simultaneously at two separate locations. Droplet coalescence was investigated over a range of carrier fluid flow rates and laser intensities. The experimental results agreed well with the theoretical models. A biodegradable gel microparticle was continuously synthesized. The microbiodegradable particles offer a useful technology in medical and drug delivery applications (Sugiura et al. 2005). Calcium alginate has been the most frequently used in those applications for its usability in fabrication process. The present results may be implemented in a variety of transparent microfluidic chips, such as polymers, glass capillaries, and polydimethylsiloxane, which permit rapid prototyping for the development of biological assays.

2 Experimental

Figure 1a shows a schematic diagram of the optofluidic droplet coalescence system. Two types of droplets were

Fig. 1 **a** Schematic illustrations of the optofluidic droplet coalescence device. **b** Microfluidic channel description. The two water droplets were generated via the T-junction geometry and were transported to the coalescence region. The flow rate in the main channel was varied without altering the droplet size by introducing a sheath flow through the microbridge structure. **c** The droplet coalescence process is illustrated as occurring in three steps. In the optical beam region, the droplet was trapped at the position in which the optical force balanced the drag force. The subsequent droplet then contacted the trapped droplet. Two droplets merged to allow the reagents to react, and the larger droplet escaped the optical trap as the drag force dominated the optical trapping force



directed toward an optical trap: The first droplet stopped at the center of the laser beam under the optical gradient force, which pulled the transparent object to the center of the beam in the radial direction. The second droplet approached and coalesced with the first. The high-refractive index droplet in the low-refractive index medium was forced to remain trapped within the laser beam focal volume.

The Gaussian optical trap was formed using the beam of a Nd:YAG 1,064 nm laser (Advanced Optowave), with a power measured using a laser power meter (PHIR, Nova Display), as shown in Fig. 1. The light path and an objective lens were carefully aligned using an IR imaging card (Melles Griot Inc.). An infrared light pass filter (Edmund Optics, Inc.) and a dichroic mirror (Thorlabs, Inc.) were inserted to direct the optical ray path in the microscopy system (Olympus IX71). The dichroic mirror was used to deflect infrared wavelength light only. The laser beam was subsequently focused using an objective lens (Olympus, NA = 0.45, 20 \times). The motions of the droplets were recorded using a sCMOS camera (Neo sCMOS, Andor) at 100 frames per second. A multiport syringe pump (Nemesys Centoni GmbH) was used to control the flow rates of the working fluids.

Figure 1b shows a schematic diagram of a microfluidic chip bearing five fluidic ports (four inlets and one outlet) with mechanical filters after the inlet ports to prevent channel clogging. Two types of droplets were generated at a cross-shaped fluid junction and were directed to the test region. The width of the cross-shaped junction was 20 μm , and the height was 50 μm . The test region was 500 μm in width, and the microchannel height was 90 μm to lower the drag force on the droplets. In this study, the droplet coalescence conditions were varied by tuning the droplet velocity and laser intensity to map out a coalescence phase diagram. The flow rate of the carrier fluid was adjusted via the sheath flow rate through a microbridge structure to adjust the interval between droplets. The droplet size remained constant as the net flow rate was adjusted by changing the sheath flow using the microbridge (Lee et al. 2011). The droplet coalescence regimes were explored by holding the droplet size constant as the drag force and optical gradient force were varied.

A transparent PDMS microfluidic chip was fabricated using standard soft lithography processes. The polymer was formed by mixing a PDMS base and a curing agent (Sylgard 184, Dow Corning) at a weight ratio of 10:1 and pouring onto the already developed photoresist pattern (Su-8 2050, Microchem) after UV exposure on a silicon wafer. The water-in-oil droplet formation required that the inner surface of the microfluidic chip be hydrophobic. Silane containing fluorocarbon liquid (EGC-1720, 3M) was gently flowed through the flow cell and dried

at room temperature to render the surface hydrophobic. The droplet stability was increased by using HFE-7500 ($\text{C}_7\text{F}_{15}\text{OC}_2\text{H}_5$, $n = 1.29$, 3M) with 40 v/v% 1H,1H,2H,2H-perfluoro-1-octanol ($\text{C}_8\text{H}_5\text{F}_{13}\text{O}$, $n = 1.313$, Sigma Aldrich) as the continuous phase fluid. Heavy water (D_2O , Sigma Aldrich) containing 4 M CaCl_2 ($n = 1.4234$) was used as the dispersed phase fluid to prevent light absorption from the Nd:YAG 1,064 nm laser (Lee et al. 2012). We found that the absorption rate from the laser beam was very small since the residence time of the droplet in the illumination of the laser beam was the order of few hundreds of milliseconds (Dholakia and Reece 2006). An alginic acid sodium salt solution (3 wt%, Sigma Aldrich) in heavy water was used as the dispersed phase fluid that, in the presence of the calcium chloride (CaCl_2) in a second set of dispersed phase droplets present in the device, formed particles. As an application of the droplet coalescence method, Ca-alginate beads were synthesized using the experimental setup.

3 Results and discussion

The droplet coalescence procedure is schematically illustrated in Fig. 1c. The droplets passed through the light beam, and the optical gradient force pulled the droplet toward the beam center along the radial direction. If the optical force acting on the droplet were sufficient to overcome the drag force, the droplet was trapped. The subsequent droplet then came into contact with the trapped droplet and merged with the optical trap through collisions. The coalesced droplet escaped the optical trap once the drag force began to dominate the optical gradient force as the droplet size increases.

The droplet behavior was investigated numerically by estimating the forces acting on the droplet. Several hydrodynamic forces (inertial, lift, buoyancy, gravity, drag, etc.) and external forces (optical scattering and gradient) acted on the droplet within the microfluidic channel. Among these forces, the drag and optical forces were dominant. The inertial migration and wall lift forces negligibly affected the droplet migration because the Reynolds number was not sufficiently high. Apart from the optical and drag forces, the buoyancy force was not taken into account for the theoretical characterization of the droplet motion. The droplets were assumed to remain a spherical shape during the trapping and coalescence. Each droplet had a radius of 25 μm , much larger than the wavelength of the laser beam (1,064 nm). For this reason, the ray optics regime could be used to calculate the momentum transfer from the light beam to the droplet. Kim and Kim (2006) have analyzed the optical forces that act on a particle in a microfluidic channel. The optical gradient and scattering forces can be expressed as

$$F_g = \frac{n_1 r_d^2}{2c} \int_0^{2\pi} \int_0^{\pi/2} I(\rho, z) Q_g \sin 2\theta_1 \cos \varphi d\theta_1 d\varphi, \quad (1)$$

$$F_s = \frac{n_1 r_d^2}{2c} \int_0^{2\pi} \int_0^{\pi/2} I(\rho, z) Q_s \sin 2\theta_1 d\theta_1 d\varphi, \quad (2)$$

where F_g is the optical gradient force, and F_s is the optical scattering force, respectively. Here, c denotes the speed of light in a vacuum, n_1 is the refractive index of the fluid medium, and r_d is the droplet radius. $I(\rho, z)$ is the beam intensity profile, where ρ and z are the radial and axial displacements, respectively, from the beam center to the center of the droplet. Q_g and Q_s are defined as dimensionless coefficients of momentum change for a single photon along the radial (gradient force) and axial (scattering force) directions.

On the other hand, the droplet size was not small enough to ignore the flow profile around the droplet. The Stokes drag force, which has been used to estimate the drag force exerted on a particle, was modified (Jung et al. 2014) as

$$F_d = 6\pi \mu^* r_d (k_1 u_\infty - k_2 u_d), \quad (3)$$

where F_d is the drag force, μ^* is the effective viscosity, and u_∞ is the velocity of the fluid at the same streamline in the absence of the droplet. u_d is the droplet velocity, which is calculated at every time step. The effects of the two viscous fluids (a water droplet in oil) flowing together inside the microchannel were estimated by considering the viscosity of the dispersed and continuous phase fluids. The effective viscosity could be represented as

$$\mu^* = \mu_c \frac{1 + 2\mu_c/3\mu_d}{1 + \mu_c/\mu_d}, \quad (4)$$

where μ_c is the continuous phase fluid viscosity, and μ_d is the disperse phase fluid viscosity, respectively. k_1 and k_2 in Eq. (3) are the drag coefficients and depend on the droplet size, displacement, and geometry of the microfluidic channel (Jung et al. 2014). The coefficient k_1 accounts for a stationary droplet in a uniformly flowing carrier fluid, whereas k_2 represents a moving droplet in a quiescent fluid. The coefficients may be derived using the analytic solutions described in a previous study of the drag forces acting on a droplet near a single plate and extrapolated those solutions to the system of droplets flowing inside the microchannel (van der Sman 2010).

By calculating the optical and drag forces, the behaviors of the droplets could be predicted according to

$$m_d \frac{du_d}{dt} + F_d = F_g, \quad (5)$$

where m_d is the droplet mass. The droplet behavior is shown in Fig. 2. The 25 μm droplet flowed through the

microchannel with a total flow rate of 155 $\mu\text{L/h}$. Figure 2a shows the displacement of droplets in the x-direction for laser powers of 2, 3, and 4 W. The droplets accelerated at around 20 ms and decelerated a few ms later under the optical gradient force. A laser power of 2 and 3 W decelerated the droplets within the optical trap, but did not trap the droplets. For an input power of 4 W, the droplet was successfully trapped at a specific position along the x-direction. The red curve corresponds to a trapped droplet, whereas the black and blue curves correspond to droplets that escaped the optical trap. Note that the escaped droplet formed under the former conditions (black curve) dwelled longer in the optical trap compared with the later conditions (blue curve).

The moving droplets' momentum ($p = m_d u_\infty$) was defined by multiplying the droplet mass (m_d) and velocity (u). The droplets were trapped by bringing the net momentum of the droplets to zero as the droplet reached a standstill position in the optical trap. The magnitude of the momentum decrease ($\Delta p = p_1 + p_2$) was equivalent to the integral over the net force (drag plus optical) with respect to time. The change in momentum should be equal to this value but opposite in direction to the momentum of the moving droplet prior to entering the optical trap. This essential condition for droplet trapping and later coalescence may be stated as:

$$m_d u_\infty = \int_{t_1}^{t_2} (F_d + F_g) dt = -(p_1 + p_2), \quad (6)$$

where p_1 and p_2 are the momentum added to the droplet in the acceleration and deceleration zones (where p_2 is negative). For droplet trapping, it is important that the momentum sum ($p_1 + p_2$), such that $|p_2| > |p_1|$, should be equal and opposite to $m_d u_\infty$. The droplet momentum change may be quantitatively estimated by plotting the optical gradient force and drag force over time, as shown in Fig. 2b, c. The force distributions are shown as a function of time, and the inset figure shows the force distribution as a function of the droplet displacement along the flow direction. The positive peak in Fig. 2b immediately prior to 20 ms indicated that the droplet accelerated prior to approaching the laser beam center. A dip in the curve immediately after 20 ms indicated that the droplet decelerated as it flowed past the light beam center. At this stage, the droplet could escape or remain in the optical trap, depending on the laser intensity. At laser powers of 2 or 3 W, the optical force on the droplet decreased dramatically as the droplet was moved away from the beam center. For a laser power of 4 W, the intensity was sufficiently high to trap the droplets, and the optical and drag forces were balanced.

The drag force acting on the droplet over time and the displacement in the x-direction are shown in Fig. 2c. The drag force resisted the acceleration and deceleration of the

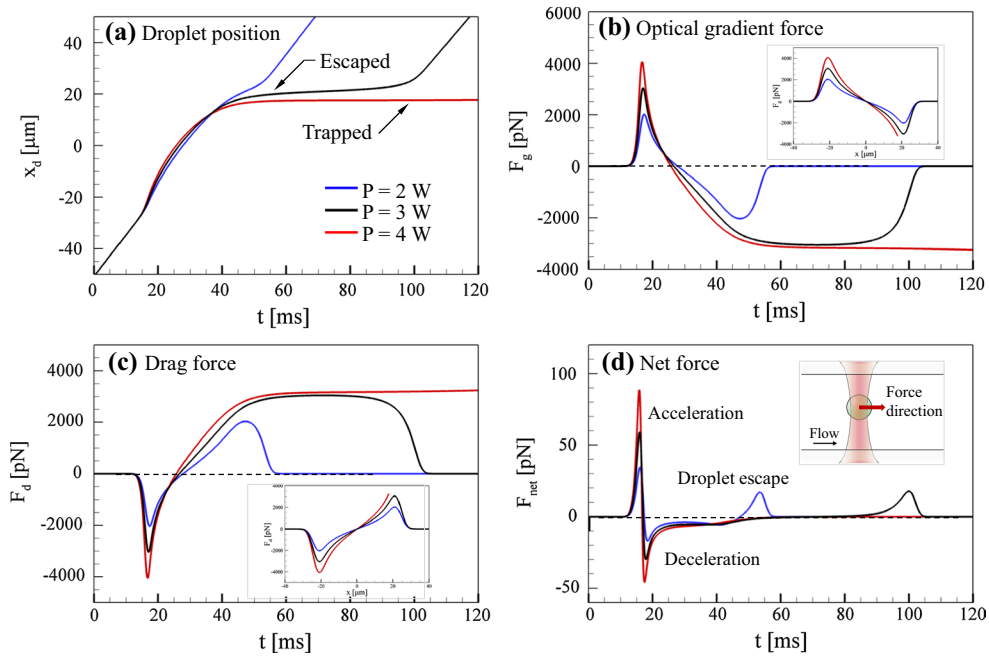


Fig. 2 Numerical predictions of the droplet positions and force distribution. A flow rate of 155 $\mu\text{L/h}$ and laser intensities of 2, 3, and 4 W were used with droplets of radius 25 μm . The droplet position change in the x-direction (fluid flow direction) (a), the calculated optical gradient force (b), the drag force on the droplets in the microfluidic channel (c), and the net force acting on the droplets (d) versus time are plotted. The force on the droplet was specified as positive when aligned along the flow direction. The optical beam pulling the droplets toward its center accelerated + the droplet as it approached

the center and decelerated the droplet as it moved away. The local maxima of the net force that pushed the droplets along the flow direction exceeded the net force that pulled the droplets along the opposite direction. The time during which the droplet resided within the deceleration region was much longer than the time during which the droplet resided within the accelerating region due to droplet deceleration. The total momentum transfer applied to the droplets trapped the droplets. The inset graphs in b and c show the optical gradient force and the drag force versus the x-axis droplet position

droplets in the fluid flow. The magnitude of the drag force was comparable to the optical gradient force and acted to oppose the optical force. The droplet carried some momentum before entering the laser beam. The net momentum transfer from photons to the droplet should be equal opposite to the flow direction to ensure droplet trapping. The optical gradient force was responsible for the droplet acceleration and deceleration in the optical trap and produced an indirect drag force that acted on the droplet. The net force could be reasonably calculated by summing up the optical gradient force and the drag force. The net force acting on the droplet, a direct result of optical trap, was plotted as a function of time in Fig. 2d. The positive values of the net force corresponded to droplet acceleration, whereas the negative values suggested deceleration. The area under the curves could be regarded as the momentum transferred to the droplet from the optical laser beam. The area associated with the positive net force indicated momentum added to the droplet along the flow direction, whereas the opposite was true for a negative net force.

In the trapped droplet case (red curve), the magnitude of the first local maxima of the net force exceeded the magnitude of the local minima; however, the momentum

added along the flow direction was much lower than the momentum transferred opposite to the flow direction, as the deceleration time was much longer than the acceleration time. The area under the curve in the droplet acceleration zone (12–15 ms) was lower, as was the momentum addition (p_1), than the corresponding area in the deceleration zone (15–53 ms) [and the oppositely directed momentum addition (p_2)]. It could be inferred that $|p_2| > |p_1|$, and the net momentum addition from the photons was sufficient to counterbalance the initial momentum (p) of the droplet. The initial droplet acceleration and deceleration in the cases of the escaped droplet (black and blue curves) were similar to the profiles of the trapped droplet case; however, the net momentum addition could only slow down the droplet, which eventually yielded to the drag force imposed by the fluid flowing past the droplet. The secondary maximum offered an explanation for why the droplet escaped the trap at 53 ms and 100 ms for input powers of 2 and 3 W, respectively. At 2 W (blue curve), the droplet resided for a short time in the optical trap compared with the case when the input power was 3 W (black curve). The escaped droplet acquired the lost momentum (p) by acquiring the flow velocity u_∞ . The calculation results revealed that trapping

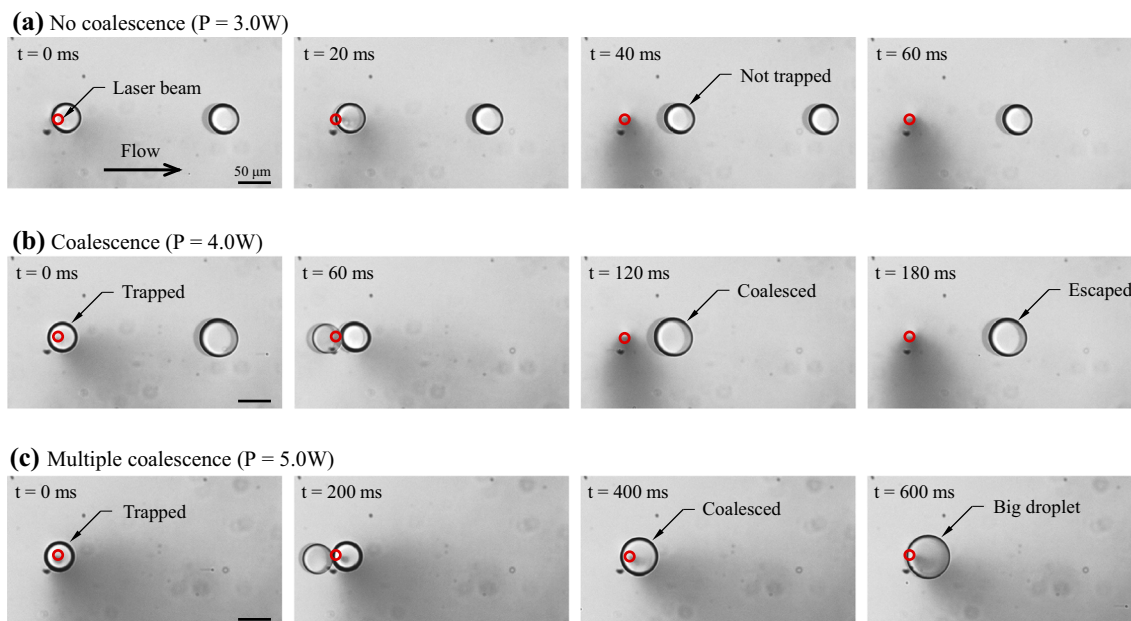


Fig. 3 Representative images of the droplet trapping and coalescence processes in the microfluidic channel. The droplet coalescence regimes could be categorized as: **a** no coalescence, **b** coalescence, and **c** multiple coalescence. The laser intensities were 3, 4, and 5 W, respectively

was possible if the laser power exceeded 4 W under the experimental conditions used here.

The experimental results are shown in Fig. 3 and the ESI movie I. The droplet coalescence regime was evaluated using only one type of droplet. Particle synthesis was demonstrated using two different types of droplets. The water droplet flow rate was $0.5 \mu\text{L/h}$, and the oil flow rate was $50 \mu\text{L/h}$. The total flow rate was controlled by varying the sheath flow rate through the microbridge channel from 75 to $180 \mu\text{L/h}$ while holding the laser power at 2, 3, 4, or 5 W. Three cases of droplet coalescence under a total flow rate of $155 \mu\text{L/h}$, and 3, 4, and 5 W laser powers are shown in Fig. 3 and the ESI movie I. The droplets were transported to the right and trapped by the laser beam marked as a red circle.

Experimentally, the droplet coalescence process could be categorized according to three regimes: no coalescence, coalescence, and multiple coalescence events. The droplet trajectories were recorded using a sCMOS camera while the droplet passed through the laser beam. The droplets slowed down under the optical gradient force. Figure 3a shows that the droplet escaped from the optical trap before reaching a complete stop because the sum of the momentum transfer from the photons did not exceed the kinetic momentum of the droplet. Figure 3b shows the droplet coalescence induced by the optical trapping. The droplet stopped within the optical trap, while another droplet approached to coalesce upon collision. Coalescence was achieved without emulsification stabilizers. The larger droplets generated were dominated by the drag force and escaped the optical trap after merging.

These results agreed well with the numerical predictions illustrated in Fig. 2. The merged droplets remained stationary as the laser power was increased to 5 W (Fig. 3c). The already trapped coalesced droplets merged again with the upstream droplets. These results enabled us to estimate the input power for a specific flow rate in the microchannel so as to avoid the undesired conditions that led to multiple coalescence events.

Figure 4 shows a phase diagram of droplet coalescence, generated to characterize the droplet trapping and

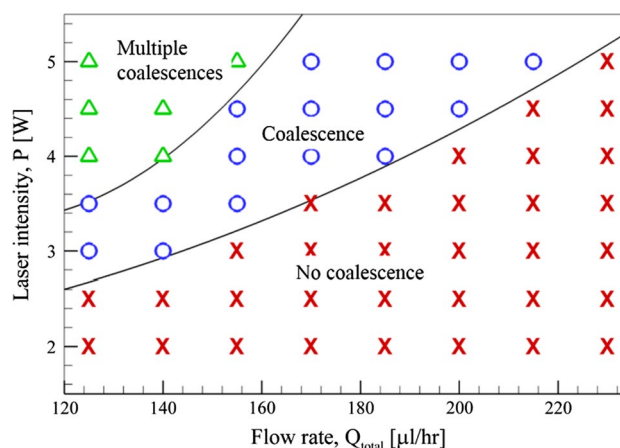
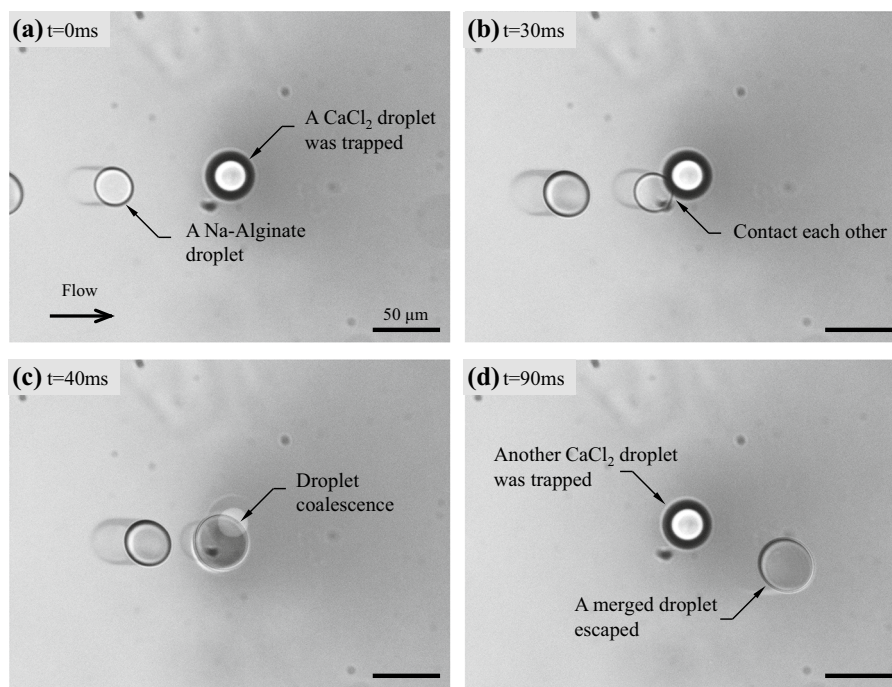


Fig. 4 A phase diagram showing the droplet coalescence under the optical forces in the microfluidic channel, under various conditions. The symbols in the figure represent the experimental results: no coalescence (cross), coalescence (circle), and multiple coalescence (triangle) (color figure online)

Fig. 5 Production of the biodegradable calcium alginate gel microparticles via the optofluidic droplet coalescence system. The channel height was $80\ \mu\text{m}$, the laser intensity was $5\ \text{W}$, and the total flow rate used to generate and transport the droplets was $240\ \mu\text{L/h}$. A $4\ \text{M}\ \text{CaCl}_2$ solution in heavy water ($0.2\ \mu\text{L/h}$) and an alginic acid sodium salt solution in heavy water ($0.2\ \mu\text{L/h}$) were used as the droplet contents. **a** The CaCl_2 droplet was trapped by the optical trapping. The CaCl_2 droplets and Na-alginate droplets were generated in pairs. **b** The droplets came in contact. **c** The droplets successfully merged and mixed. **d** The merged droplet escaped from the optical trap, and another droplet was trapped again



coalescence properties experimentally. The droplet coalescence regimes were classified and marked as no coalescence (cross), coalescence (circle), and multiple coalescence events (triangle). The experimental results indicate that transition lines could be drawn to identify the droplet merging regime. The phase diagram revealed that the number of droplets to be coalesced in a microfluidic channel could be controlled precisely by varying the laser intensity or flow rate.

Biodegradable calcium alginate gel microparticles were synthesized using the optofluidic droplet coalescence method proposed above. The synthesis procedure is illustrated in Fig. 5 and shown in the ESI movie I. In this experiment, the microfluidic channel height was $80\ \mu\text{m}$, the oil flow rate was $240\ \mu\text{L/h}$, and the laser intensity was $5\ \text{W}$. A $4\ \text{M}\ \text{CaCl}_2$ solution in heavy water ($0.2\ \mu\text{L/h}$) and an alginic acid sodium salt solution in heavy water ($0.2\ \mu\text{L/h}$) were used as two different dispersed phases to generate the droplet. The two types of droplets were generated in pairs in the same microfluidic channel and were later coalesced. Figure 5a shows that the droplet containing CaCl_2 was trapped by the optical force, and the Na-alginate-containing droplet followed behind. After 30 ms, the droplets came in contact and exerted pressure against the droplet surface (Fig. 5b). Figure 5c shows that the droplets successfully merged after colliding. After coalescence, the two reactive components that had been encapsulated within separate droplets mixed under the secondary flow inside the droplets to form gel microparticles. The large merged droplet escaped the optical trap under the high drag force imposed

by the continuous phase fluid (Fig. 5d). It is important to note that only the CaCl_2 -based droplets were characterized by a refractive index that differed sufficiently from that of the oil medium to permit trapping by the optical gradient force. The Na-alginate-based droplet alone was not captured by the trap because it was characterized by a lower refractive index difference. These results were obtained several times, and the gel microparticles were synthesized continuously.

4 Conclusions

The present study demonstrated droplet trapping and coalescence under the optical forces in the microfluidic channel. The droplets were generated using a cross-shaped junction and were carried to the test section. The laser beam was incorporated within the microscopy setup to manipulate the droplets in the microchannel using an optical trap. As the optical trap captured the first droplet, the upstream droplet approached to collide and coalesce with the trapped droplet, generating a larger droplet. After coalescence, the drag force acting on the merged droplet increased due to the larger droplet size. A drag force that exceeded the optical force pushed the droplets out of the optical trap and transported them to the outlet. The droplet behavior was examined using a theoretical model of the droplets as a single rigid sphere. The numerical predictions agreed well with the experimental results. The experimental conditions were varied to identify conditions that led to no

coalescence, coalescence, or multiple coalescence events among droplets. The flow rate and laser intensity could be adjusted to readily control the droplet coalescence. This technique was used to continuously synthesize the biodegradable gel particles by merging CaCl_2 droplets and the alginic acid sodium salt droplets.

Acknowledgments This work was supported by the Creative Research Initiatives Program (No. 2014-001493) of the National Research Foundation of Korea (MSIP).

References

- Abate AR, Hung T, Mary P, Agresti JJ, Weitz DA (2010) High-throughput injection with microfluidics using picoinjectors. *Proc Natl Acad Sci USA* 107:19163–19166
- Ahn K, Agresti J, Chong H, Marquez M, Weitz DA (2006) Dielectrophoretic manipulation of drops for high-speed microfluidic sorting devices. *Appl Phys Lett* 88:264105
- Ashkin A, Dziedzic JM (1971) Optical levitation by radiation pressure. *Appl Phys Lett* 19:283–285
- Baroud CN, de Saint Vincent MR, Delville JP (2007) An optical toolbox for total control of droplet microfluidics. *Lab Chip* 7:1029–1033
- Baroud CN, Gallaire F, Dangla R (2010) Dynamics of microfluidic droplets. *Lab Chip* 10:2032–2045
- Chang SC, Su YC (2010) On-demand micro-encapsulation utilizing on-chip synthesis of semi-permeable alginate-PLL capsules. *Microfluid Nanofluid* 10:1165–1174
- Christopher GF, Bergstein J, End NB, Poon M, Nguyen C, Anna SL (2009) Coalescence and splitting of confined droplets at microfluidic junctions. *Lab Chip* 9:1102–1109
- Churski K, Kaminski TS, Jakiela S, Kamysz W, Baranska-Rybak W, Weibel DB, Garstecki P (2012) Rapid screening of antibiotic toxicity in an automated microdroplet system. *Lab Chip* 12:1629–1637
- Dholakia K, Cizmar T (2011) Shaping the future of manipulation. *Nat Photonics* 5:335–342
- Dholakia K, Reece P (2006) Optical micromanipulation takes hold. *Nano Today* 1:18–27
- Grier DG (2003) A revolution in optical manipulation. *Nature* 424:810–816
- Hoang PH, Park H, Kim DP (2011) Ultrafast and continuous synthesis of unaccommodating inorganic nanomaterials in droplet- and ionic liquid-assisted microfluidic system. *J Am Chem Soc* 133:14765–14770
- Hung LH, Choi KM, Tseng WY, Tan YC, Shea KJ, Lee AP (2006) Alternating droplet generation and controlled dynamic droplet fusion in microfluidic device for CdS nanoparticle synthesis. *Lab Chip* 6:174–178
- Jung JH, Lee KH, Lee KS, Ha BH, Oh YS, Sung HJ (2014) Optical separation of droplets on a microfluidic platform. *Microfluid Nanofluid* 16:635–644
- Kim SB, Kim SS (2006) Radiation forces on spheres in loosely focused Gaussian beam: ray-optics regime. *J Opt Soc Am B* 23:897–903
- Kotz KT, Gu Y, Faris GW (2005) Optically addressed droplet-based protein assay. *J Am Chem Soc* 127:5736–5737
- Lee DH, Lee W, Um E, Park JK (2011) Microbridge structures for uniform interval control of flowing droplets in microfluidic networks. *Biomicrofluidics* 5:34117–341179
- Lee KH, Kim SB, Yoon SY, Lee KS, Jung JH, Sung HJ (2012) Behavior of double emulsions in a cross-type optical separation system. *Langmuir* 28:7343–7349
- Lorenz RM, Edgar JS, Jeffries GD, Zhao Y, McGloin D, Chiu DT (2007) Vortex-trap-induced fusion of femtoliter-volume aqueous droplets. *Anal Chem* 79:224–228
- Luong TD, Nguyen NT, Sposito A (2012) Thermocoalescence of microdroplets in a microfluidic chamber. *Appl Phys Lett* 100:254105
- Niu X, Gulati S, Edel JB, deMello AJ (2008) Pillar-induced droplet merging in microfluidic circuits. *Lab Chip* 8:1837–1841
- Song H, Chen DL, Ismagilov RF (2006) Reactions in droplets in microfluidic channels. *Angew Chem Int Ed* 45:7336–7356
- Srinivasan V, Pamula VK, Fair RB (2007) An integrated digital microfluidic lab-on-a-chip for clinical diagnostics on human physiological fluids. *Lab Chip* 4:310–315
- Sugiura S, Oda T, Izumida Y, Aoyagi Y, Satake M, Ochiai A, Ohkohchi N, Nakajima M (2005) Size control of calcium alginate beads containing living cells using micro-nozzle array. *Biomaterials* 26:3327–3331
- Tan YC, Ho YL, Lee AP (2006) Droplet coalescence by geometrically mediated flow in microfluidic channels. *Microfluid Nanofluid* 3:495–499
- Teh SY, Lin R, Hung LH, Lee AP (2008) Droplet microfluidics. *Lab Chip* 8:198–220
- Tewhey R, Warner JB, Nakano M, Libby B, Medkova M, David PH, Kotsopoulos SK, Samuels ML, Hutchison JB, Larson JW, Topol EJ, Weiner MP, Harismendy O, Olson J, Link DR, Frazer KA (2009) Microdroplet-based PCR enrichment for large-scale targeted sequencing. *Nat Biotechnol* 27:1025–1031
- Theberge AB, Mayot E, El Harrak A, Kleinschmidt F, Huck WT, Griffiths AD (2012) Microfluidic platform for combinatorial synthesis in picolitre droplets. *Lab Chip* 12:1320–1326
- Um E, Rha E, Choi SL, Lee SG, Park JK (2012) Mesh-integrated microdroplet array for simultaneous merging and storage of single-cell droplets. *Lab Chip* 12:1594–1597
- van der Sman RG (2010) Drag force on spheres confined on the center line of rectangular microchannels. *J Colloid Interface Sci* 351:43–49
- Whitesides GM (2006) The origins and the future of microfluidics. *Nature* 442:368–373